https://doi.org/10.5194/egusphere-2026-342
Preprint. Discussion started: 25 February 2026

The MISR Research Product Algorithm – Producing Global, Self-Consistent, Pixel-Level Aerosol Retrievals for the Multi-angle Imaging SpectroRadiometer

Michael Anstett [1,2], James A. Limbacher[3,4], and Ralph A. Kahn[5,6]

[1]Science Systems and Applications, Inc., Lanham MD 20706
[2]NASA Goddard Space Flight Center, Greenbelt MD 20771
[3]Science and Technology Corporation (STC), Hampton, VA
[4]National Oceanic and Atmospheric Administration, College Park MD 20740
[5]Laboratory for Atmospheric & Space Physics, University of Colorado Boulder, Boulder CO 80303
[6]Senior Research Scientist Emeritus, NASA Goddard Space Flight Center, Greenbelt MD 20771

Correspondence to: Ralph A. Kahn (ralph.kahn@lasp.colorado.edu)

Abstract. The MISR Research Aerosol retrieval algorithm (RA) was developed in parallel with the MISR standard operational algorithm (SA), to explore innovative retrieval ideas for possible implementation in the SA, and to provide higher-spatial-resolution results with enhanced sensitivity to particle properties, where possible. Whereas the SA was designed to run automatically on the entire MISR dataset, the RA, a research code, had to be run on a case-by-case basis, with considerable user involvement. We present here a version of the RA, the MISR Research Product Algorithm (MRPA), that has been streamlined and automated for wider use, along with validation results for this algorithm. The compromises required to automate the RA result in somewhat diminished particle-type sensitivity. However, the MRPA provides 1.1 km pixel resolution (compared to 4.4 km for the SA), and comparing the AOD data statistically with AERONET, it offers about half the statistical RMSE, significantly higher correlation coefficient, though somewhat higher bias, for mid-visible AOD compared to the SA over land, along with better Ångström exponent statistics, especially at higher AOD. Statistical validation of particle shape and single-scattering albedo is more difficult, but for sufficiently high AOD, retrievals in smoke-dominated regions show a preponderance of small-medium, spherical, light-absorbing particles, whereas dust-dominated regions tend to have larger, weakly absorbing, non-spherical particles.

1 Introduction

As one of five instruments flying aboard Terra, the flagship spacecraft of NASA's Earth Observing System, MISR has been collecting radiance data since late February 2000. Despite Terra performing constellation exit procedures in October 2022, beginning the last phase of its operational lifespan, MISR will leave a legacy of collecting multi-angle, multi-spectral views of Earth for over 24 years. MISR is a push-broom swath imager that observes Earth at nine view angles (70.5, 60.0, 45.6, 26.1 in the forward and aft directions along the flight path, plus nadir), taking radiance data in four spectral bands (centered at 446, 558, 672, 866 nm) (Diner et al., 1998), and covering the globe about once a week. As a multi-angle satellite imager, MISR is better able to constrain aerosol particle microphysical properties than single-view imagers, spurring the development of algorithms to retrieve aerosol type as well as aerosol optical depth (e.g., Martonchik et al., 1998; 2009; Kahn et al., 2001; Diner et al., 2005; Kahn & Gaitley, 2015). The concept for an inherently multi-angle aerosol retrieval algorithm for MISR over-land observations was developed pre-launch, utilizing empirical orthogonal functions in view angle to characterize the contribution of the surface to top-of-atmosphere (TOA) reflectance (Diner and Martonchik 1984a; 1984b). This method serves as the basis of the over-land part of the MISR aerosol Standard Algorithm (SA), which generates the operational aerosol data product for MISR. Version 23

https://doi.org/10.5194/egusphere-2026-342
Preprint. Discussion started: 25 February 2026

of the Standard Algorithm currently retrieves aerosol amount and type information at 4.4km horizontal resolution (Garay et al., 2020).

The potential of multi-angle imaging to retrieve microphysical properties of climatogically probable aerosols was established in early sensitivity studies (Kahn et al., 1997; 1998; 2001; Limbacher & Kahn, 2014). The goal of enhancing particle microphysical property retrievals for MISR became the basis for developing the MISR Research Algorithm (RA), initially an over-water retrieval algorithm. Notable innovations and refinements to the RA include corrections to MISR reflectances for radiometric calibration error such as flat-field anomalies and ghosting in high contrast scenes (Limbacher and Kahn, 2015), and enhanced performance in scenes of shallow, turbid, and biologically productive waters (Limbacher and Kahn, 2017, 2019). This effort culminated in an algorithm capable of retrieving aerosol amount and type over land and water at a 1.1km resolution, with the capability of prescribing surface reflectance (Limbacher et al., 2022), a feature performed manually early in the RA's life (e.g., Chen et al., 2008), now done automatically in parallel with the retrieved-surface algorithm. Over-land, surface reflectances for the prescribed-surface approach are sourced from the Multi-Angle Implementation of Atmospheric Correction (MAIAC) surface albedo and reflectance dataset (Lyapustin et al., 2018, Lyapustin and Wang, 2018), derived from the NASA's MODerate resolution Imaging Spectroradiometer (MODIS) instrument. A Lambertian reflectance assumption is made to prescribe surface reflectance over water. The addition of this prescribed surface allows for aerosol information to be directly retrieved using a Bounded-Variable-Least-Squares (BVLS) approach, improving results in high-aerosol-optical-depth (AOD) cases, where retrieving the surface reflectance is difficult. This helps to mitigate a persistent low bias in high-AOD cases present in the SA (Kahn et al., 2010, Kahn and Gaitley, 2015), as well as in early versions of the RA. The inclusion of the Retrieved-Surface Algorithm (RSA), which performs better at lower AOD, and the Prescribed Surface Algorithm (PSA) in the high-AOD regime, results in the Combined Surface Algorithm (CSA), leveraging the strengths of both algorithms (Limbacher et al., 2022).

As the culmination of work on the MISR Research Algorithm, we have developed a deliverable MISR Research Product Algorithm (MRPA) to generate RA-quality aerosol particle property results for general users. It is more automated and streamlined than earlier versions of the MISR RA, and it can retrieve aerosol amount and type spanning MISR's operational lifetime in the nominal Terra orbit, from February 2000 through October 2022. The MRPA originates from the RA, principally similar to the algorithm described in Limbacher et al. (2022), with modifications to the RSA surface reflectance shape-similarity coefficient retrieval and mixture weighting, as well as an updated methodology for the over-land CSA, as detailed below. We introduce new cloud masking, interpolated to the MISR swath from the MAIAC AOD cloud mask (Lyapustin, A., 2023) where MAIAC has coverage, and include a test derived from comparing brightness temperature calculated from MODIS-Terra emission in the 12 micron band (MCST, 2017) to reanalysis sea surface temperature from the Modern-Era Retrospective analysis for Research and Applications, Version 2 (MERRA-2; GMAO, *tavg1_2d_ocn_Nx*) over deep ocean. Column ozone, used in band absorption radiance corrections, is now sourced from MERRA-2 (GMAO, *inst1_2d_asm_Nx*).

Validation of AOD and Ångström exponent (ANG) is performed against AErosol RObotic NETwork (AERONET) direct-sun photometer measurements (Holben et al., 1998). We also present a comparative analysis of aerosol property quantities including single-scattering albedo (SSA) and Fine-mode-fraction (FMF), against AERONET almucantar inversion retrievals. We include all available MISR-AERONET coincidences during the study period in this analysis. Sect. 2 presents a brief overview of the current MRPA, including changes to the RSA introduced since Limbacher et al. (2022). It continues with a description of the methodology used for validating the MRPA against AERONET. Sect. 3 presents detailed validation results and comparison against MISR-AERONET coincidences as well as against expectation for dust-dominated and wildfire-smoke-dominated cases; conclusions and closing remarks given in Sect. 4.

https://doi.org/10.5194/egusphere-2026-342
Preprint. Discussion started: 25 February 2026

2 Methodology

As the MRPA is similar to the RA described in Limbacher et al. (2022), the general description of the methodology here is brief, focusing more on introducing the changes to the algorithm version that is described in detail in that paper.

2.1 Brief algorithm description, highlighting updates

MISR raw radiances are converted to reflectances, with corrections for stray light, flat-fielding, temporal trends in the radiometric calibration, out-of-band sensitivity and ozone absorption, all performed as part of pre-processing (Limbacher and Kahn, 2014; 2015; 2017; 2019). MISR radiances are available past October 2022. A new version of the MISR Level 1 radiance data is being generated, using dynamic orbit processing to account for the Terra satellite's subsequent orbit drift; back-processing for the preceding 22 years is planned. However, the MRPA currently is configured to process only data up to October 2022, to maintain continuity with the correction approach in the RA. The PSA methodology is unchanged; over land, Ross-Thick Li-Space (RTLS) surface bi-directional reflectance factor (BRF) kernels from MAIAC Collection 6 (Lyapustin et al., 2018; Lyapustin and Wang, 2018) are temporally and spatially interpolated to the MISR swath at overpass time. Over-water, we assume Lambertian reflectance typical of dark water (0.0257, 0.00668, 0.00093, 0.0000635 in the four MISR spectral bands, respectively). When the surface reflectance is prescribed externally, aerosol quantities can be calculated directly using a bounded-variable least squares (BVLS) retrieval approach. In the current implementation, the RSA, which retrieves surface reflectance self-consistently along with aerosol quantities, uses a shape similarity assumption (e.g., Diner et al., 2005), whereby the angular shape of the surface reflectance is taken as independent of wavelength:

$$\mathrm{BRF}^{\mathrm{Surf}}_{\lambda,c} = \mathrm{A}^{*}_{\lambda} \times \mathrm{B}_{c}\,;\, A^{*}_{\lambda} = \frac{A_{\lambda}}{1 - s_{\lambda} \times A_{\lambda}} \qquad (1)$$

where A^{*}_{λ} represents a modified surface albedo, defined in terms of the view-invariant surface albedo A_{λ}, and the effective atmospheric backscatter, s_{λ}, and B_{c} represents the spectrally invariant angular brightness (i.e., the shape similarity) coefficient, with subscript *c* representing the MISR camera index (Limbacher et al., 2022, *Eq. (5)*). The cost function is then expressed in terms of B_{c} and this modified surface albedo, A^{*}_{λ} (Limbacher et al., 2022, *Eq. (6)*). Over water, the shape similarity coefficient is set to 1.0 (i.e., the Lambertian assumption) and solving for the modified surface albedo, A^{*}_{λ} (Limbacher et al., 2022, *Eq. (7)*), is sufficient to determine surface reflectance. For the over-land retrieval, B_{c} must be determined as well. Previously, the calculation of B_{c} used BRFs from all four MISR bands (Limbacher et al., 2022, *Eq. (8)*). As the NIR tends to penetrate the atmosphere better than the shorter MISR spectral bands, the new shape similarity coefficient calculation uses exclusively values from the NIR band:

$$B_{c} = \frac{\frac{w_{NIR,c}}{Unc^{2}_{NIR,c}} \times TT_{NIR,c} \times A^{*}_{\mathrm{NIR}} \times \left[BRF^{TOA}_{NIR,c} - BRF^{Path}_{NIR,c}\right]}{\frac{w_{NIR,c}}{Unc^{2}_{NIR,c}} \times \left[TT_{NIR,c} \times A^{*}_{\mathrm{NIR}}\right]^{2}} \qquad (2)$$

Here $w_{NIR,c}$ represent weights assigned to each channel, *TT* is the surface-to-camera transmittance, *Unc* is the channel radiometric uncertainty, and BRF^{TOA} and BRF^{Path} are the top-of-atmosphere BRF and the contribution of the atmosphere to the TOA BRF, respectively. This approach generally allows for better constraint on the surface reflectance, especially compared to including the green and blue bands.

https://doi.org/10.5194/egusphere-2026-342
Preprint. Discussion started: 25 February 2026

In the RSA, normalized mixture weights are calculated once the optimum AOD and surface reflectance for each mixture have been derived. In the previous version of the RA, mixture weights were calculated as follows:

$$MW_m = \frac{exp\left(\frac{Cost_{min}-Cost_m}{Cost_{min}+0.01}\right)}{\sum_m [exp\left(\frac{Cost_{min}-Cost_m}{Cost_{min}+0.01}\right)]} \quad (3)$$

where m represents aerosol mixture, $Cost_m$ is the lowest cost for each of the 104 mixtures (defined in Table S1 in Supplemental Material), and $Cost_{min}$ represents the lowest cost among all mixtures (Limbacher et al., 2022, *Eq. (9)*). Weighted aggregate parameters are then calculated for AOD, mixture fraction, and surface reflectance characteristics. In the MRPA, mixture weights are now calculated according to:

$$MW_m = \frac{100\,\hat{}\left(\frac{Cost_{min}-Cost_m}{Cost_{min}+0.01}\right)}{\sum_m 100\hat{}\,[\left(\frac{Cost_{min}-Cost_m}{Cost_{min}+0.01}\right)]} \quad (3b)$$

and used to calculate weighted aggregate parameters in the same way. This change adds weight to mixtures having lower values of the cost function difference ratio, meaning that few mixtures will contribute to the weighting. A description of the quality flags used for the over-land and over-water retrievals is given in Supplemental Material.

2.2 Updated over-land combined surface algorithm methodology

The PSA performs poorly over bright regions such as desert, where small errors in the prescribed surface reflectance can create large errors in the retrieved aerosol. Accordingly, over-land, the CSA used by the MRPA is weighted more heavily, based on the Normalized Difference Vegetation Index (NDVI), obtained from the MAIAC-derived prescribed surface albedo. Specifically, in Limbacher et al. (2022), results from the CSA were weighted according to:

$$CSA = RSA * w_0 + PSA * w_1, \quad (4)$$

where w_0 was defined as:

PSA AOD < 0.75	$w_0 = 1$
0.75 < PSA AOD < 1.5	$w_0 = 1 - \frac{PSA\ AOD-0.75}{1.5-0.75}$
PSA AOD > 1.5	$w_0 = 0$

and the relationship between w_0 and w_1 is

$$w_0 = 1 - w_1. \quad (5)$$

For the MRPA, we follow the previous method and use the NDVI as before, but we introduce updated weighting terms based on results from the extensive validation dataset developed here,

$$CSA = RSA * w'_0 + PSA * w'_1 \quad (6)$$

Where the following is enforced for w'_0, and the relationship in Eq. (5) is maintained:

NDVI < 0.10	$w'_0 = 1$
0.10 < PSA AOD < 0.25	$w'_0 = 1 - \frac{NDVI-0.10}{0.25-0.10} * w_0$
NDVI > 0.25	$w'_0 = w_0$

https://doi.org/10.5194/egusphere-2026-342
Preprint. Discussion started: 25 February 2026

2.3 External datasets for inputs and cloud masking

As with previous versions of the RA, we prescribe 10-meter wind speeds for ocean surface roughness estimation from the Cross-Calibrated Multiplatform (CCMP) v2.0 ocean surface wind velocity data (Mears et al., 2019). These wind speeds are spatially interpolated to the MISR swath and temporally interpolated from 6-hour increments to MISR overpass time. To maintain a continuous source of column ozone spanning MISR's lifetime, which is used to account for ozone absorption in the MISR channels, we now incorporate column ozone in Dobsons from the MERRA-2 reanalysis (GMAO, *inst1_2d_chm_Nx*). Column ozone values from MERRA-2 are obtained from the nearest 6-hourly measurement and interpolated to the MISR swath at coarse resolution (17.6km x 17.6km).

For better cloud masking over land, we use the 1km cloud mask from the MODIS-Terra MAIAC AOD data product (Lyapustin, A., 2023). We establish a matrix where MAIAC pixels masked as cloud or near-cloud are given a value of 1.0, and clear pixels are set as zero. This matrix is then linearly interpolated from the MAIAC sinusoidal grid to the MISR swath. Resultant values greater than zero are masked as cloud. We apply the same methodology to the MAIAC AOD product land mask, for better constraint on surface conditions during validation. As MAIAC only retrieves sinusoidal tiles containing land, for cloud masking over deep ocean, we calculate brightness temperature from MODIS-Terra emission band 32 at 12 mm (MCST, 2017), and spatially interpolate it to the MISR grid. We then compare this against MERRA-2 sea-surface temperature, where pixels with an emission brightness temperature exceeding the sea-surface temperature by 7.5K are masked as cloud. Both the land and ocean cloud masks are propagated across- and along-track to mitigate against stereoscopic and cloud motion effects introduced by going from MODIS datasets to MISR.

2.4 Validation methodology using AERONET

AERONET sun photometers provide direct measurements of spectral AOD from hundreds of sites around the world (Holben et al., 1998), with an uncertainty around 0.01, verified by periodic reference calibration (Eck et al., 1999; Sinyuk et al., 2012). Ångström exponent is also reported accurately, so long as spectral AOD is greater than 0.1-0.2 (Wagner and Silva, 2008). We use AERONET Version 3, level 1.5 (L1.5) AODs, which provide many more coincidences with MISR than level 2, and far better cloud masking and retrieval accuracy than level 1 (Giles et al., 2019). We interpolate spectral AOD from four AERONET bands (1020nm, 870nm, 675nm, and 440nm) to the four MISR bands using a second-order polynomial in log space. We calculate Ångström exponent (446-870nm) as the negative slope of the line fitting these spectral AODs to their respective wavelengths in log-log space. Spectral AODs acquired within ±30 minutes of the MISR overpass at each site are averaged for these calculations.

AERONET almucantar inversions (Dubovik and King, 2000) provide ground-based retrievals of column-effective particle single-scattering albedo (SSA), fine-mode fraction (FMF), and sphericity, that can be compared with the MRPA results. However, unlike the spectral AOD values, which are retrieved from direct-sun measurements, there are important caveats to the AERONET inversion variables, including FMF and sphericity (e.g., Kahn & Gaitley, 2015). For example, the AERONET definition of fine mode changes with each inversion, as mode separation is determined based on the minimum in retrieved AOD vs. particle size in each retrieval. For non-sphericity, an ANG threshold is applied, so the non-spherical fraction is forced to be coarse-mode dominated, even though transported dust can be dominated by fine mode. And the same indices of refraction are adopted for all components in the atmospheric column; if there are several distinct aerosol types having different refractive indices in the column, such as a transported dust layer over near-surface pollution particles, the size and SSA inversion results will be skewed. As such, ANG derived from the direct-sun measurements is a much more robust variable for validating the MISR particle-size-related values than reported "effective sizes" from MISR or AERONET. Further, at low AOD, the inversion

https://doi.org/10.5194/egusphere-2026-342
Preprint. Discussion started: 25 February 2026

variables, especially SSA, are less certain. The assumptions made are required, due to the inherent limitations in passive, total-column remote-sensing measurements, whether they are made from the surface or from orbit. We take these factors into account in what follows, by considering the *validation* of MISR RA results against direct-sun AERONET spectral AOD ground truth, as distinct from *comparisons* between MISR RA and AERONET inversion variables.

We average the following quantities: absorbing AOD, fine-mode AOD, coarse-mode AOD (each in the 440, 675, 870, and 1020nm bands), and sphericity over a ±4-hour window surrounding MISR overpass time, as almucantar retrievals are sampled less frequently than direct-sun AODs. These quantities are each interpolated to 550nm, with FMF calculated as fine-mode AOD/(fine-mode AOD + coarse-mode AOD), and SSA defined as 1.0 – (absorbing AOD)/(fine-mode AOD + coarse-mode AOD).

2.5 MRPA analysis by aerosol source

We present additional analysis for cases likely to be dominated by a single aerosol type during certain seasons – biomass burning and dust. We select an assortment of AERONET sites in locations and in months where a single aerosol type is dominant. These broadly include regions in forested area and shrubland in local summer throughout the world for biomass-burning, especially where wildfires are historically prevalent at those times. Dust-dominated regions are selected from sites in and around desert regions, particularly surrounding the Sahara Desert in late spring and early summer. The general expectation is that biomass burning aerosol will be dominated by small-medium, spherical, somewhat light-absorbing particles, and dust aerosol, at least near-source, will be dominated by larger, non-spherical, weakly light-absorbing particles in most cases. A list of the selected sites and months for each aerosol type is included in the supplemental material (Table S2).

3.1 MRPA over-land validation against AERONET

Using the averaging and interpolation methodology described in Sect. 2 yields 69,191 MISR-AERONET sun photometer over-land coincidences out of all available sites from February 2000 to October 2022. Figure 1 displays plots of MISR vs AERONET mid-visible AOD from the RSA, PSA, and CSA. The retrieved surface produces more consistent results at low AOD whereas the prescribed surface approach performs better at high AOD, as explained in Sect. 1 above. Figure 2 presents the 68th percentile | CSA AOD – AERONET AOD | error, plotted against CSA AOD. Data are binned in increments of 2% of the total data. The fit of these data in Fig. 2 is used to generate the expected AOD error envelope of CSA AOD ± (CSA AOD * 0.17 – 0.01), i.e., a measure of the spread of points around the 1:1 line as a function of AOD. Table S3 in the supplement contains the statistical results of the comparison of the three algorithms vs. AERONET.

As in Limbacher et al. (2022), the approach of combining the output of the RSA and the PSA produces improved statistics for AOD over land. In Fig. 1C, the retrieved AOD appears to fit the AERONET validation data well. The statistics, presented in Table S3, show quantitatively that the CSA reports 9% lower RMSE for AOD than the RSA, and an improved correlation coefficient. Note that the RSA is applied toward lower AOD (Limbacher et al., 2022), and the number of validation cases is also skewed toward lower AOD values; due to this weighting, the CSA results are closer to the RSA than the PSA results overall. However, Fig. 1D does show that at higher AOD, the CSA reports greater values of AOD than the RSA, displaying the influence of the PSA mixing in. For total CSA statistics against AERONET, RMSE is 0.083 (Table S3) compared to 0.154 for the MISR V23 standard product (Garay et al., 2020), the Bias is 0.008 for the CSA compared to -0.002 for the standard product, and the correlation coefficient r is 0.941 compared to 0.81 for the standard product. Note that the CSA and V23 standard product comparison datasets are not identical, but in both cases thousands of cases are included, covering a globally extensive range of locations, using similar MISR-AERONET coincidence criteria.

https://doi.org/10.5194/egusphere-2026-342
Preprint. Discussion started: 25 February 2026

Figure 3 shows plots of MISR ANG (466-867nm) compared against AERONET for various MISR CSA AOD thresholds. Table S4 in the supplement gives the comparison statistics associated with Fig. 3, including the results reported by the RSA, PSA and CSA individually. As shown in Figures 1 and 3, and Tables S3 and S4, the CSA reports AOD and ANG with less error and bias than the RSA and PSA, so subsequent analysis for the over-land results refers exclusively to the CSA. The plots within Fig. 3 display two clusters of ANG values, around 0.25 and 1.5, that reflect the general clustering of coarse-mode and fine-mode aerosol sizes, respectively, and likely correspond to dust-dominated scenes and smoke/pollution-dominated scenes, respectively. Figure 3(B) suggests that at lower AOD, the ANG corresponding to coarse-mode may be biased high relative to AERONET, whereas fine-mode-dominated scenes are better retrieved. These deviations are reduced at higher AOD, as shown in Fig. 3(C). Improved particle property retrieval results at higher AOD is well established (e.g., Kahn & Gaitley, 2015; Limbacher et al., 2022), as the aerosol signal/noise generally increases with increased AOD. Again, comparing with the MISR V23 standard product (Garay et al., 2020) as best we can, RMSE for the CSA decreases from 0.43 to 0.25 with increasing AOD threshold (Table S4); for the V23 standard product overall, RMSE is 0.45, though the data are not stratified by AOD threshold. The CSA Bias ranges from -0.096 to +0.143, generally decreasing with increasing AOD, whereas the V23 standard product reports 0.002 overall, and for CSA AOD > 0.2, r ranges from 0.76 to 0.89, compared to 0.71 overall for the V23 standard product.

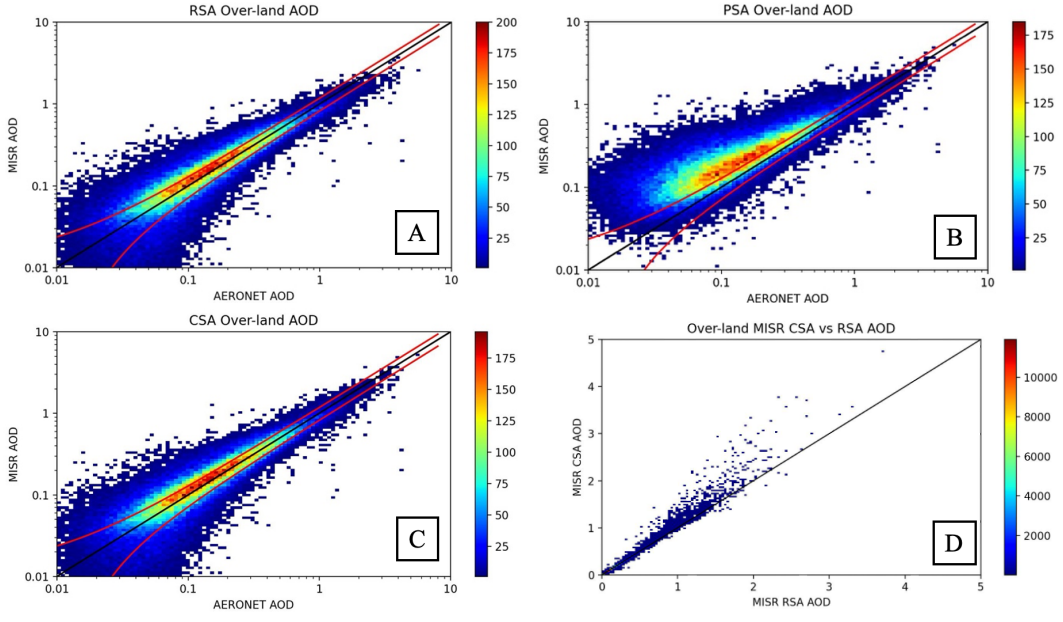

Figure 1: Comparison of MRPA 550nm AOD retrievals vs. AERONET direct-sun 550nm AOD for all available over-land MISR_AERONET coincidences between February 2000 and October 2023. The x axis of each plot displays AERONET AOD, whereas the y axis represents MISR AOD. For easier viewing of points at lower values of AOD, data are plotted as a 2D histogram with log-log axes. Panel (A) shows retrieved-surface algorithm (RSA) AOD, (B) displays prescribed-surface algorithm (PSA) AOD, and (C) displays the combined-surface algorithm (CSA) AOD. Panel (D) shows over-land MISR CSA AOD vs MISR PSA AOD, plotted in linear space, with the x axis representing MISR RSA AOD and the y axis representing MISR CSA AOD. The black lines represent one-to-one agreement, and the red lines embedded in each plot display the expected combined-surface algorithm (CSA) error envelope of MISR CSA AOD ± (0.17 * CSA AOD + 0.01). Statistics associated with this figure are given in Table S3 in the supplement.

https://doi.org/10.5194/egusphere-2026-342
Preprint. Discussion started: 25 February 2026

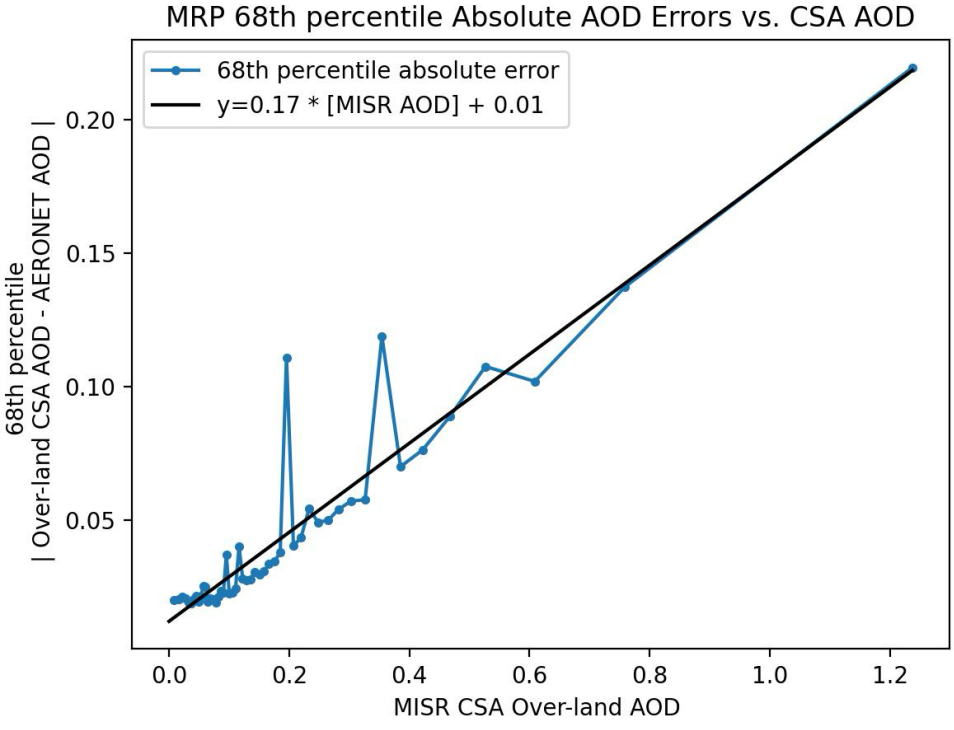

Figure 2: 68th percentile | CSA over-land 550nm AOD - AERONET 550nm AOD | error vs CSA AOD. Points are binned at 2% of total coincidences (roughly 1515 coincidences per bin). The fit of these data is used to derive the expected error envelope of 0.17*(CSA AOD) + 0.01, which the black line represents.

https://doi.org/10.5194/egusphere-2026-342
Preprint. Discussion started: 25 February 2026

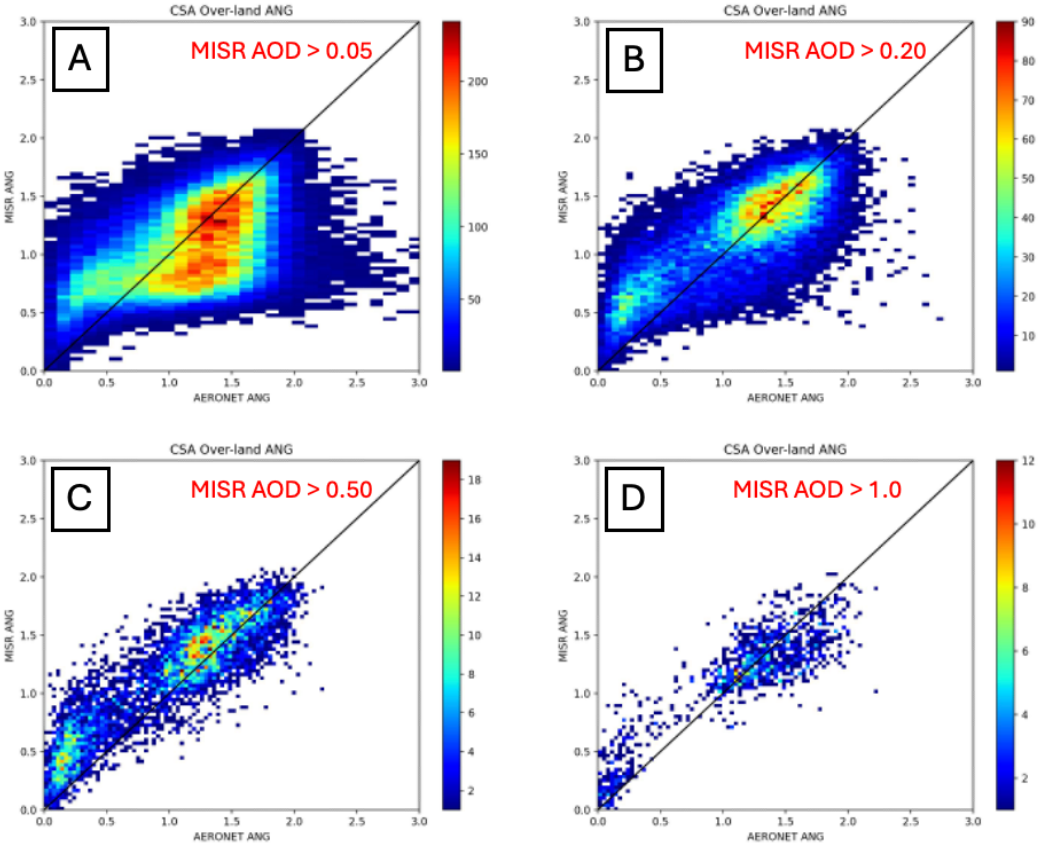

Figure 3: Plots of over-land MISR combined-surface Ångström exponent against AERONET Ångström exponent (446-867nm). Data are plotted as 2D histograms, with the x axes as AERONET Ångström exponent and the y axes as MISR CSA-retrieved Ångström exponent. Each plot displays data constrained by a different lower bound of CSA AOD, indicated by the red text. The black lines represent a one-to-one agreement between MISR and AERONET. Statistics associated with this figure are given in Table S4 in the supplement.

We present RA particle property results compared against AERONET inversion data Fig. 4 presents 550nm AOD FMF and SSA for CSA AOD > 1. Using the flagging methodology described in the supplement and the ± 4h averaging window for AERONET inversion data yields 795 coincidences when AOD > 1. Table S5 in the supplement contains the statistics corresponding to these results. They are qualitatively comparable to previous studies of MISR particle-property retrieval sensitivity (e.g., Kahn and Gaitley, 2015). On a global basis, there is a preponderance of fine-mode aerosol, with a secondary peak at approximately 80% coarse-mode; the retrieved mode-separation becomes clearer with increasing AOD. The size-mode separation is supported by, and consistent with, the more robust validation of ANG shown in Fig. 3. Retrieved SSA is rarely lower than 0.9. Quantitative assessment of the FMF and SSA results is more difficult to achieve due to inherent limitations of the AERONET inversion results, as discussed in Sect. 2.4 above. As such, we also rely on data over regions and at times when dust or smoke dominate the atmospheric aerosol load to perform further validation of CSA particle property retrieval results (Sect. 3.3 below).

https://doi.org/10.5194/egusphere-2026-342
Preprint. Discussion started: 25 February 2026

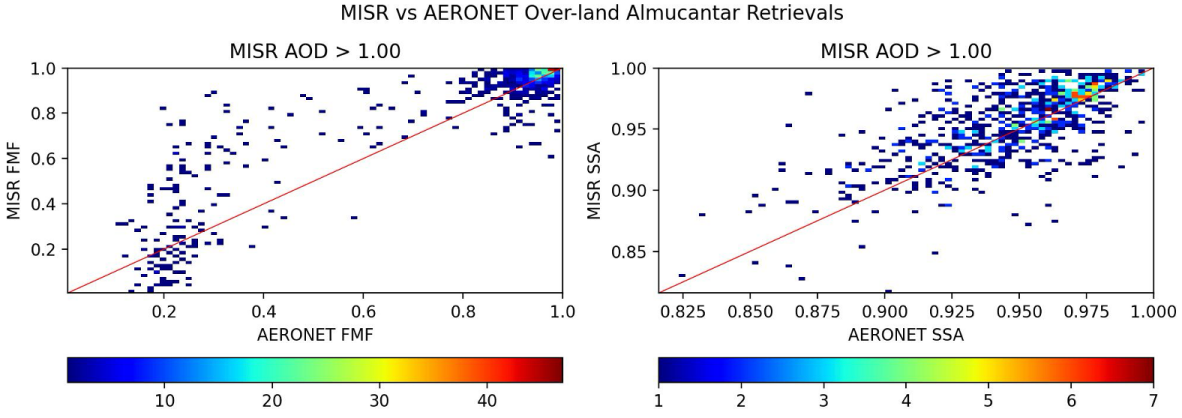

Figure 4: Plots of MISR vs. AERONET 550nm over-land fine-mode-fraction (FMF), and 550 nm single-scattering-albedo (SSA). Results correspond to cases for MISR AOD > 1.0. Results are plotted as 2D histograms, with the x and y axes representing AERONET and MISR results, respectively. The left plot represents FMF, and the right plot represents SSA. The embedded red lines represent one-to-one agreement of AERONET to MISR. Statistics associated with this figure are given in Table S5 in the supplement.

3.2 MRPA over-water validation against AERONET

Figure 5 presents our assessment of the MISR RSA, PSA, and CSA AOD performance relative to AERONET direct-sun measurements over ocean. Given the geographical distribution of AERONET sites, there are there are 62% fewer over-water MISR-AERONET coincidences in the validation dataset. However, with almost 24 years of once-weekly global data in the study set, the more than 26,000 over-water coincidences are ample to provide robust statistics. Given the preponderance of low-AOD cases over ocean, the RSA and CSA statistics are nearly identical. The CSA over-water RMSE relative to coincident AERONET data is 0.063, the bias is 0.009, and r is 0.093 (Table S6); the corresponding values over land are 0.083, 0.088, and 0.941 (Table S3), respectively. The uncertainty of AOD retrievals over dark water tends to be lower than over land, but the generally lower absolute values of AOD over water tend to compensate for the difference in the aggregated statistics. The expected over-water CSA error analysis results, which are nearly identical to that over land (Fig. 2 above), is assessed as Fig. S1 in the supplement.

https://doi.org/10.5194/egusphere-2026-342
Preprint. Discussion started: 25 February 2026

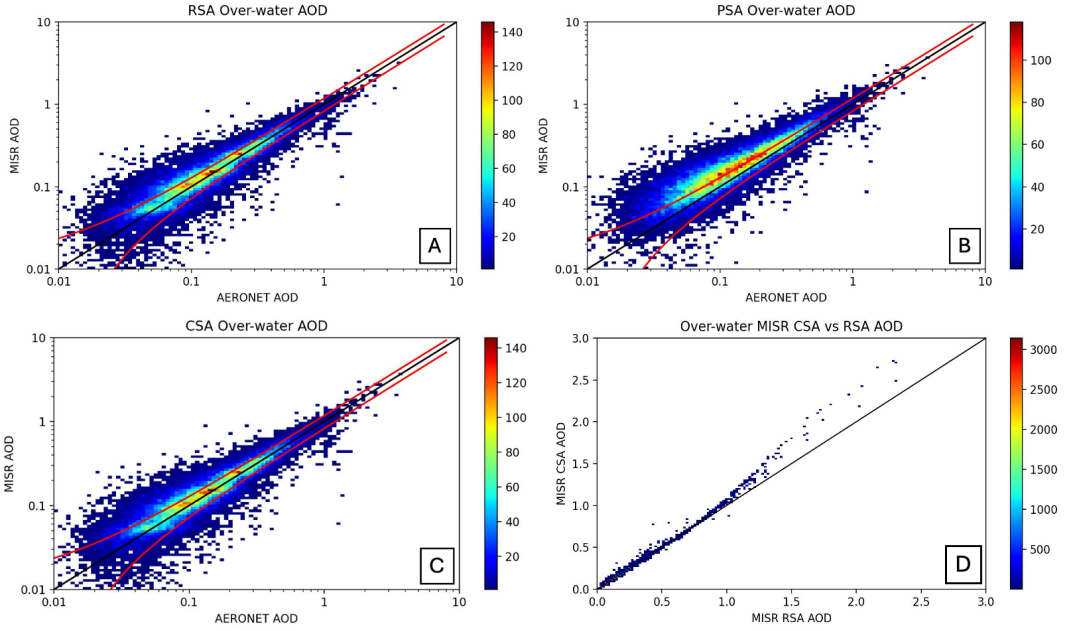

Figure 5: Comparison of over-water MRPA 550nm AOD retrievals vs. AERONET direct-sun 550nm AOD for all available MISR-AERONET coincidences between February 2000 and October 2023. The x axis of each plot displays AERONET AOD, whereas the y axis represents MISR AOD. Data are plotted as a 2D histograms with log-log axes. Panel (A) shows retrieved-surface algorithm (RSA) AOD, (B) displays prescribed-surface algorithm (PSA) AOD, and (C) displays the combined-surface algorithm (CSA) AOD. Panel (D) shows over-land MISR CSA AOD vs MISR PSA AOD, plotted in linear space, with the x axis representing MISR RSA AOD and the y axis representing MISR CSA AOD. The black lines represent one-to-one agreement, and the red lines embedded in each plot display the expected over-water combined-surface algorithm (CSA) error of MISR CSA AOD ± (0.16 * CSA AOD + 0.01). Statistics associated with this figure are given in Table S6 in the supplement.

Ångström exponent comparisons with coincident AERONET direct-sun values over water, stratified by CSA AOD, are shown in Fig. 6, and the associated statistics are given in Table S7 in the supplement. As with the over-land results, the data cluster around a fine and a coarse mode, with the fine mode dominating. As might be expected, over-water results compare favorably with AERONET, relative to the over-land results, when stratified by AOD. For example, for AOD > 0.20, with over 24,000 points, the CSA over-water ANG RMSE relative to coincident AERONET data is 0.293, the bias is 0.012, and r is 0.849; the corresponding values over land are 0.337, 0.055, and 0.760 (Table S4), respectively.

https://doi.org/10.5194/egusphere-2026-342
Preprint. Discussion started: 25 February 2026

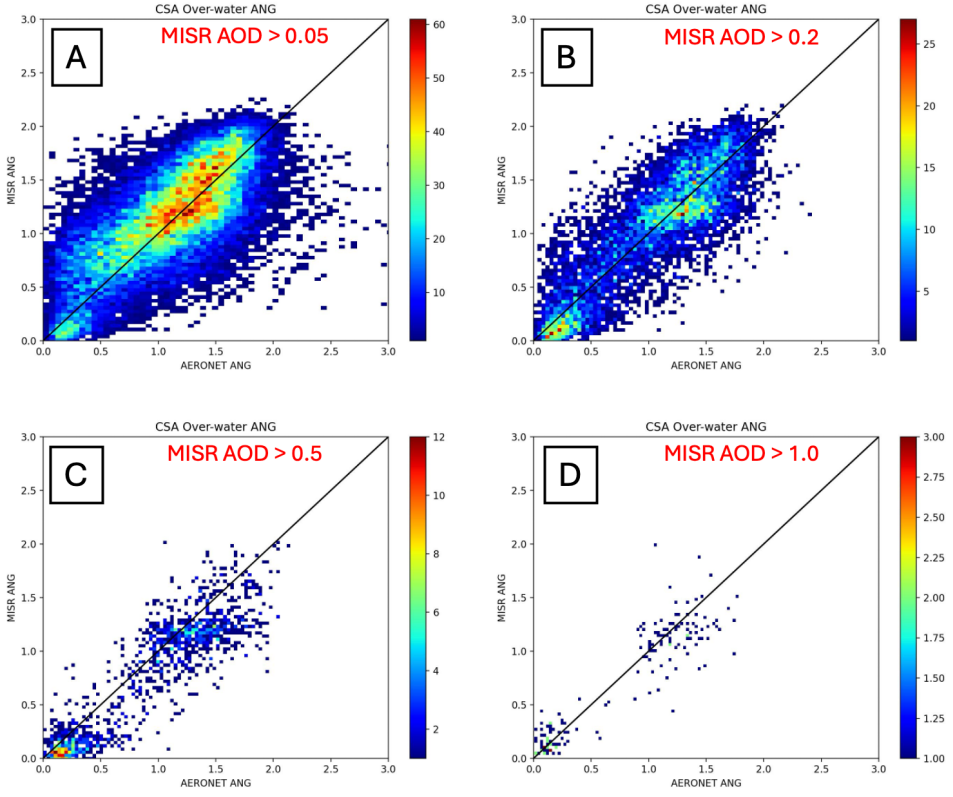

Figure 6: Plots of over-water MISR combined-surface Ångström exponent against AERONET Ångström exponent (446-867nm). Data are plotted as 2D histograms, with the x axes as AERONET Ångström exponent and the y axes as MISR CSA-retrieved Ångström exponent. Each plot displays data constrained by a different lower bound of CSA AOD, indicated by the red text. The black lines represent one-to-one agreement between MISR and AERONET. Detailed statistics associated with this figure are given in Table S7 in the supplement.

Figure S2 and Table S8 in the supplement offer a comparison between CSA and AERONET FMF of 550 nm AOD, and SSA at 550 nm, over water. As expected, there are fewer coincidences over water than over land (Table S4). For comparable AOD strata, there are again distinct fine- and coarse-mode clusters; the FMF over-water correlations are higher, whereas the RMSE and bias statistics are similar to those over land. Also similar to the over-land results, the SSA correlations are very poor due to extreme clustering at SSA values near unity; as such, the leverage of relatively few lower-SSA points skews the linear fitting. However, the RMSE and bias are low, as the CSA and AERONET agree that the preponderance of SSA values fall near unity for this data cohort.

3.3 MRPA Properties for Smoke- and Dust-Dominated Cases

As discussed in Sect. 2.4, there are relatively few MISR-AERONET coincidences where a significant smoke or dust plume is within the field-of-view of both instruments. In this section, we explore available MISR-AERONET coincidences in our validation dataset during months and in regions where either wildfire smoke plumes or mineral dust plumes generally occur, with the understanding that not all cases will actually be smoke- or dust-dominated. As such, this is just a qualitative assessment of particle-type discrimination trends, but it is about the best we can do statistically with the current dataset. Quantitative assessments have been published elsewhere, using the RA for individual smoke (e.g., Junghenn Noyes et al., 2020a; 2020b;

https://doi.org/10.5194/egusphere-2026-342
Preprint. Discussion started: 25 February 2026

Junghenn Noyes & Kahn, 2024) and dust or volcanic ash (e.g., Flower & Kahn, 2020a; 2020b; Kahn & Limbacher, 2025; Yue et al., 2022) cases, where either coincident aircraft field validation data was available or specific, known plumes were sampled. Figures 7 and 8 present the CSA-retrieved ANG, FMF, SSA, and Non-Sph as a function of CSA AOD for sites most likely to be smoke-dominated and dust-dominated, respectively. The AERONET site names and specific months selected are given in Tables S2.1 and S2.2 in supplemental material for smoke and dust, respectively. Despite the scatter due to sampling uncertainty, when the mid-visible AOD exceeds about 0.2 over water and about 0.7 over land, the smoke retrievals are predominantly fine-mode dominated, whereas at least over water, where retrieval signal/noise is highest, the dust cases are distinctly coarse-mode dominated, and ANG is close to zero.

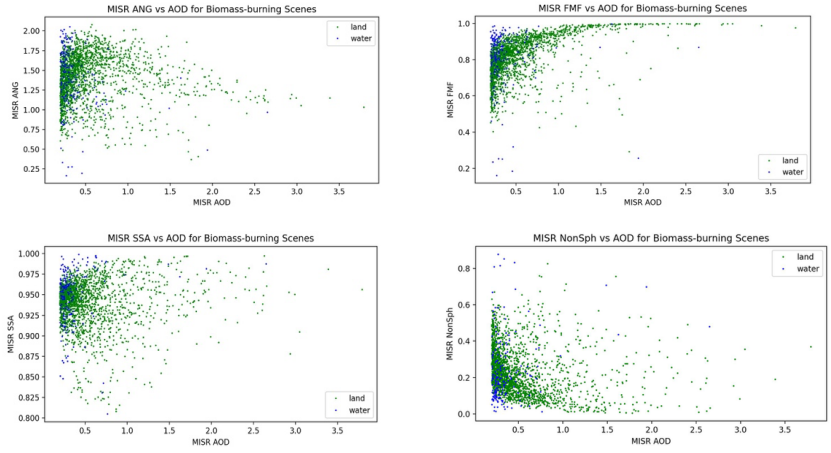

Figure 7: Plots of MISR CSA-retrieved: (a) ANG, (b) FMF, (c) SSA, and (d) Non-Sph, vs. AOD, over land (green points) and water (blue points), for locations and seasons when wildfire smoke plumes are most likely to occur. (See text for selection details.)

Mid-visible SSA is between about 0.9 and 0.975 for the smoke cases (Fig. 7c), whereas for dust cases, the lower bound is distinctly higher (0.94-0.98), though the peak values are still less than unity (Fig. 8c). Non-Sph varies widely over land and at low AOD, but again, as AOD increases above ~0.5, the smoke cases are predominantly spherical (Fig. 7d) whereas the dust cases are largely non-spherical, especially over water (Fig. 8d), despite the sampling uncertainties. These are the patterns we would expect for smoke and dust, respectively, when the airmass is dominated by either species and the AOD is sufficiently high to raise the aerosol signal significantly above the surface contribution to the top-of-atmosphere reflectances.

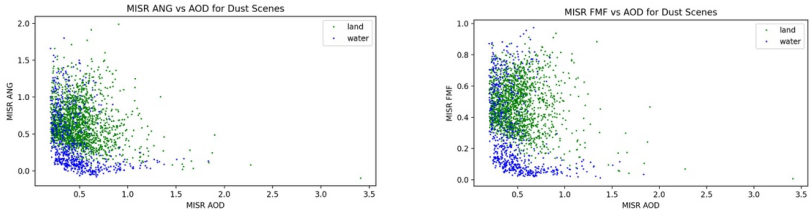

https://doi.org/10.5194/egusphere-2026-342
Preprint. Discussion started: 25 February 2026

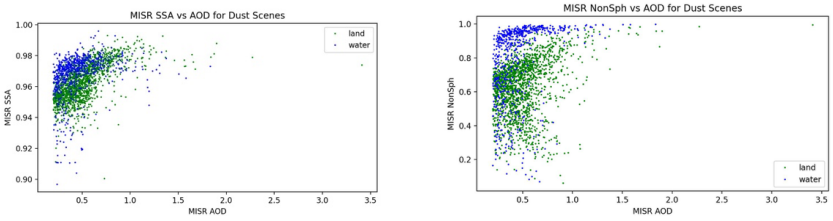

Figure 8. Plots of MISR CSA-retrieved: (a) ANG, (b) FMF, (c) SSA, and (d) Non-Sph, vs. AOD, over land (green points) and water (blue points), for locations and seasons when mineral dust plumes are most likely to occur. (See text for selection details.)

4 Conclusions

The MISR Research Aerosol retrieval algorithm (RA) was developed to explore innovative advancements that could be applied to the MISR Standard Aerosol retrieval algorithm (SA) that runs routinely on the entire MISR dataset, and to optimize the particle microphysical property information content of the retrieval results. However, as a research code, the RA requires special knowledge to run, and it was practical to apply only on limited subsets of the MISR data. We introduce here a version of the RA, the MISR Research Product Algorithm (MRPA), that has been streamlined and automated for use by the wider research community, along with validation results for this algorithm. The compromises required to automate the RA result in somewhat diminished particle-type sensitivity. However, the MRPA provides 1.1 km pixel resolution (compared to 4.4 km for the SA). Using AERONET AOD for validation, the MRPA offers about half the statistical RMSE, significantly higher correlation coefficient, though somewhat higher bias, for mid-visible AOD compared to the SA over land, along with better Ångström exponent statistics, especially at higher AOD. Statistical validation of particle shape and single-scattering albedo is more difficult, but for AOD > ~0.2 over water and > ~0.5 over land, retrievals in smoke-dominated regions show a preponderance of small-medium, spherical, light-absorbing particles, whereas dust-dominated regions tend to have larger, weakly absorbing, non-spherical particles. Quantitative validation of RA-retrieved aerosol size, shape, and light-absorption has been published elsewhere, for selected individual cases where the AOD is sufficiently high to produce adequate signal/noise for such retrievals (a rare occurrence for MISR-AERONET coincidences). Over the NASA Earth Observing System era, MISR provides a unique data record of aerosol properties globally, about once per week, along with AOD results that complement those from MODIS and other single-view instruments. The MRPA is available for general use as described in the Open Data statement of this paper.

Acknowledgements

We thank the AERONET team for making their data available and the NASA Langley Atmospheric Sciences Data Center (ASDC) for archiving the relevant MISR data. This work has been supported by a grant from the NASA Terra-Aqua-Suomi NPP program, and the NASA Earth Observing System Terra and MISR projects. The authors declare no conflicts of interest related to this work.

Financial support

This work was supported primarily by a grant from the NASA Terra-Aqua-Suomi-NPP program, under Barry Lefer. Additional support came from the NASA Earth Observing Terra and MISR projects.

https://doi.org/10.5194/egusphere-2026-342
Preprint. Discussion started: 25 February 2026

Open Data

The MISR radiance data used in this study are publicly available, and were obtained from https://asdc.larc.nasa.gov/data/MISR/. The AERONET data were obtained from https://aeronet.gsfc.nasa.gov, and the MISR MRPA is being archived publicly, posted on GitHub at https://github.com/mranst/misr_research_product_algorithm. To the extent possible, the MISR MRPA validation data will be archived at the NASA Langley ASDC.

References

Chen, W.-T., Kahn, R. A., Nelson, D., Yau, K., and Seinfeld, J.: Sensitivity of multi-angle imaging to optical and microphysical properties of biomass burning aerosols, J. Geophys. Res., 113, D10203, doi:10.1029/2007JD009414, 2008.

Diner, D. J. and Martonchik, J. V.: Atmospheric Transfer of Radiation Above an Inhomogeneous Non-Lambertian Reflective Ground. I: Theory, J. Quant. Spectrosc. Ra., 31, 97–125, 1984a.

Diner, D. J. and Martonchik, J. V.: Atmospheric Transfer of Radiation Above an Inhomogeneous Non-Lambertian Reflective Ground. II: Computational Considerations and Results, J. Quant. Spectrosc. Ra., 32, 279–304, 1984b.

Diner, D. J., Beckert, J. C., Reilly, T. H., Bruegge, C. J., Conel, J. E., Kahn, R. A., Martonchik, J.V., Ackerman, T. P., Davies, R., Gerstl, S. A. W., Gordon, H. R., Muller, J. P., Myneni, R., Sellers, R. J., Pinty, B., and Verstraete, M. M.: Multiangle Imaging SpectroRadiometer (MISR) description and experiment overview, IEEE Trans. Geosci. Remt. Sensing, 36, 1072-1087, doi: 10.1109/36.700992, 1998.

Diner, D. J., Martonchik, J. V., Kahn, R. A., Pinty, B., Gobron, N., Nelson, D. L., and Holben, D. L.: Using angular and spectral shape similarity constraints to improve MISR aerosol and surface retrievals over land. Rem. Sens. Environ., 94, 155-171, doi: 10.1016/j.rse.2004.09.009, 2005.

Dubovik, O. and King, M. D.: A flexible inversion algorithm for retrieval of aerosol optical properties from Sun and sky radiance measurements, J. Geophys. Res., 105, 20673–20696, 2000.

Eck, T. F., Holben, B. N., Reid, J. S., Dubovik, O., Smirnov, A., O'Neill, N. T., Slutsker, I., and Kinne, S.: Wavelength dependence of the optical depth of biomass burning, urban, and desert dust aerosols, J. Geophys. Res., 104, 31333–31349, https://doi.org/10.1029/1999JD900923, 1999.

Flower, V. J. B., and Kahn, R. A.: The regional volcanology of Kamchatka, based on multi-sensor satellite observations. Remt. Sens. Environ., 237, doi:10.1016/j.rse.2019.111585, 2020a.

Flower, V. J. B., and Kahn, R. A.: The evolution of Iceland volcano emissions, as observed from space. J. Geophys. Res., 125, e2019JD031625, doi:10.1029/2019JD031625, 2020b.

Garay, M. J., Witek, M. L., Kahn, R. A., Seidel, F. C., Limbacher, J. A., Bull, M. A., Diner, D. J., Hansen, E. G., Kalashnikova, O.V., Lee, H., Nastan, A. M., and Yu, Y.: Introducing the 4.4 km Spatial Resolution MISR Aerosol Products. Atm. Meas. Tech., 13, 593-628, doi.org/10.5194/amt-13-593-2020, 2020.

Giles, D. M., Sinyuk, A., Sorokin, M. G., Schafer, J. S., Smirnov, A., Slutsker, I., Eck, T. F., Holben, B. N., Lewis, J. R., Campbell, J. R.,Welton, E. J., Korkin, S. V., and Lyapustin, A. I.: Advancements in the Aerosol Robotic Network (AERONET) Version 3 database – automated near-real-time quality control algorithm with improved cloud screening for Sun photometer aerosol optical depth (AOD) measurements, Atmos. Meas. Tech., 12, 169– 209, https://doi.org/10.5194/amt-12-169-2019, 2019.

https://doi.org/10.5194/egusphere-2026-342
Preprint. Discussion started: 25 February 2026

GMAO (Global Modeling and Assimilation Office): MERRA-2 inst1_2d_asm_Nx: 2d,1-Hourly, Instantaneous, Single-Level, Assimilation, Single-Level Diagnostics V5.12.4, Greenbelt, MD, USA, Goddard Earth Sciences Data and Information Services Center (GES DISC) [data set], https://doi.org/10.5067/3Z173KIE2TPD, 2015.

GMAO (Global Modeling and Assimilation Office): MERRA-2 tavg1_2d_ocn_Nx: 2d, 1-Hourly, Time-Averaged, Single-Level, Assimilation, Ocean Surface Diagnostics V5.12.4, Greenbelt, MD, USA, Goddard Earth Sciences Data and Information Services Center (GES DISC) [data set], https://doi.org/10.5067/Y67YQ1L3ZZ4R, 2015.

Holben, B. N., et al.: AERONET—A federated instrument network and data archive for aerosol characterization, Remote Sens. Environ., 66, 1–16, 1998.

Junghenn Noyes, K. T., Kahn, R. A., Limbacher, J. A., Sedlechek, A., Kleinman, L., and Li, L.: Wildfire Plume Particle Properties and Evolution, From Space-Based Multi-angle Imaging. Biomass Burning special issue, Remote Sens., 12, 769; doi:10.3390/rs12050769, 2020a.

Junghenn Noyes, K. T., Kahn, R. A., Limbacher, J. A., Li, Z., Fenn, M. A., Giles, D. A., Hair, J. W., Katich, J. M., Moore, R. H., Robinson, C. E., Sanchez, K. J., Shingler, T. J., Thornhill, K. L., Wiggins, E. B., and Winstead, E. L.: Wildfire Smoke Particle Properties and Evolution, From Space-Based Multi-Angle Imaging II: The Williams Flats Fire During the FIREX-AQ Campaign. Remote Sens., 12, 3823, doi:10.3390/rs12223823, 2020b.

Junghenn Noyes, K. T., and Kahn, R. A.: Satellite Multi-angle Observations of Wildfire Smoke Plumes during the CalFiDE Field campaign: Aerosol Plume Heights, Particle Property Evolution, and Aging Timescales. J. Geophys. Res., 129, e2023JD039041, doi: 10.1029/2023JD039041, 2024.

Kahn, R. A., West, R., McDonald, D., Rheingans, B., and Mishchenko, M. I.: Sensitivity of Multi-angle remote sensing observations to aerosol sphericity, J. Geophys. Res., 102, 16861-16870, doi: 10.1029/96JD01934, 1997.

Kahn, R. A., Banerjee, P., McDonald, D., and Diner, D.: Sensitivity of Multiangle imaging to Aerosol Optical Depth, and to Pure-Particle Size Distribution and Composition Over Ocean, J. Geophys. Res., 103, 32,195-32,213, doi: 10.1029/98JD01752.

Kahn, R.A., P. Banerjee, and D. McDonald, 2001. The Sensitivity of Multiangle Imaging to Natural Mixtures of Aerosols Over Ocean, J. Geophys. Res., 106, 18219-18238, doi: 10.1029/2000JD900497, 1998.

Kahn, R. A., Gaitley, B. J., Garay, M. J., Diner, D. J., Eck, T., Smirnov, A., and Holben, B. N.: Multiangle Imaging SpectroRadiometer global aerosol product assessment by comparison with the Aerosol Robotic Network. J. Geophys. Res., 115, D23209, doi:10.1029/2010JD014601, 2010.

Kahn, R. A., and Gaitley, B. J.: An analysis of global aerosol type as retrieved by MISR. J. Geophys. Res. Atmos., 120, 4248-4281, doi:10.1002/2015JD023322, 2015.

Kahn, R. A., Limbacher, J. A., Junghenn Noyes, K. T., Flower, V. J. B., Zamora, L. M., and McKee, K.: Evolving Particles in the 2022 Hunga-Tonga Hunga-Ha'apai Volcano Eruption Plume. J. Geophys. Res., 129, e2023JD039041. doi:10.1029/2023JD039041, 2024.

Kahn, R. A. and Limbacher, J. A.: Particle Microphysical-Property Evolution in a North African Dust Plume During Trans-Atlantic Transport. J. Geophys. Res., 130, e2025JD043779, doi:10.1029/2025JD043779, 2025.

Limbacher, J. A. and Kahn, R. A.: MISR Research-Aerosol-Algorithm: Refinements For Dark Water Retrievals. Atm. Meas. Tech., 7, 1-19, doi:10.5194/amt-7-1-2014, 2014.

Limbacher, J. A. and Kahn, R. A.: MISR Empirical Stray Light Corrections in High-Contrast Scenes. Atmos. Meas. Tech., 8, doi:10.5194/amt-8-1-2015, 2015

https://doi.org/10.5194/egusphere-2026-342
Preprint. Discussion started: 25 February 2026

Limbacher, J. A. and Kahn, R. A.: Updated MISR dark water research aerosol retrieval algorithm – Coupled 1.1 km ocean surface Chlorophyll-a retrievals with empirical calibration corrections. Atmos. Meas. Tech., 10, 1539–1555, doi:10.5194/amt-10-1539-2017, 2017.

Limbacher, J. A. and Kahn, R. A.: Updated MISR dark water research aerosol retrieval algorithm – Part 2: Aerosol and surface-reflectance retrievals over shallow, turbid, and eutrophic water. Atmos. Meas. Tech., 12, 675–689, doi:10.5194/amt-12-675-2019, 2019.

Limbacher, J.A., Kahn, R. A., and Lee, J.: The New MISR Research Aerosol Retrieval Algorithm: A Multi-Angle, Multi-Spectral, Bounded-Variable Least Squares Retrieval of Aerosol and Surface Properties. Atmosph. Meas. Tech., 15, 6865–6887, doi:10.5194/amt-15-6865-2022, 2022.

Lyapustin, A.: MODIS/Terra+Aqua AOD and Water Vapor from MAIAC, Daily L3 Global 0.05Deg CMG V061., distributed by NASA EOSDIS Land Processes DAAC, https://doi.org/10.5067/MODIS/MCD19A2CMG.061, 2023.

Lyapustin, A. and Wang, Y.: MCD19A3 MODIS/Terra+Aqua BRDF Model Parameters 8-Day L3 Global 1 km SIN Grid V006, NASA EOSDIS Land Processes DAAC, https://doi.org/10.5067/MODIS/MCD19A3.006, 2018.

Lyapustin, A.,Wang, Y., Korkin, S., and Huang, D.: MODIS Collection 6 MAIAC algorithm, Atmos. Meas. Tech., 11, 5741–5765, https://doi.org/10.5194/amt-11-5741-2018, 2018.

Martonchik, J.V., Diner, D. J., Kahn, R. A., Verstraete, M. M., Pinty, B., Gordon, H. R., and Ackerman, T.P.: Techniques for the Retrieval of aerosol properties over land and ocean using multiangle data, IEEE Trans. Geosci. Remt. Sensing, 36, 1212-1227. doi: 10.1109/36.701027, 1998.

Martonchik, J. V., Kahn, R. A., and Diner, D.J.: Retrieval of Aerosol Properties over Land Using MISR Observations. In: Kokhanovsky, A.A. and G. de Leeuw, ed., Satellite Aerosol Remote Sensing Over Land, Springer, Berlin, 267-293, ISBN: 978-3-540-69396-3, 2009

Mears, C. A., Scott, J.,Wentz, F. J., Ricciardulli, L., Leidner, S. M., Hoffman, R., and Atlas, R.: A near-real-time version of the crosscalibrated multiplatform (CCMP) ocean surface wind velocity data set, J. Geophys. Res.-Oceans, 124, 6997–7010, 2019.

Sinyuk, A., Holben, B. N., Smirnov, A., Eck, T. F., Slutsker, I., Schafer, J. S., Giles, D. M., and Sorokin, M.: Assessment of error in aerosol optical depth measured by AERONET due to aerosol forward scattering, Geophys. Res. Lett., 39, L23806, https://doi.org/10.1029/2012GL053894, 2012.

Wagner, F. and Silva, A. M.: Some considerations about Ångström exponent distributions, Atmos. Chem. Phys., 8, 481–489, https://doi.org/10.5194/acp-8-481-2008, 2008.

Yue, J., Miller, S. D., Straka, W., Noh, Y.-J., Chou, M.-Y., Kahn, R. A., Flower, V. J. B.: La Soufriere volcanic eruptions launched gravity waves into space. Geoph. Res. Lett. 49, doi:10.1029/2022GL097952, 2022.